

Cite this: *Chem. Sci.*, 2024, 15, 3140

All publication charges for this article have been paid for by the Royal Society of Chemistry

# Frustrated Lewis pairs on pentacoordinated Al<sup>3+</sup>-enriched Al<sub>2</sub>O<sub>3</sub> promote heterolytic hydrogen activation and hydrogenation†

Qingyuan Wu,<sup>‡ab</sup> Ruixuan Qin,<sup>id</sup> ‡<sup>ac</sup> Mengsi Zhu,<sup>b</sup> Hui Shen,<sup>a</sup> Shenshui Yu,<sup>a</sup> Yuanyuan Zhong,<sup>a</sup> Gang Fu,<sup>a</sup> Xiaodong Yi,<sup>id</sup> \*<sup>a</sup> and Nanfeng Zheng,<sup>id</sup> \*<sup>ab</sup>

As an emerging class of metal-free catalysts, frustrated Lewis pairs (FLPs) catalysts have been greatly constructed and applied in many fields. Homogeneous FLPs have witnessed significant development, while limited heterogeneous FLPs catalysts are available. Herein, we report that heterogeneous FLPs on pentacoordinated Al<sup>3+</sup>-enriched Al<sub>2</sub>O<sub>3</sub> readily promote the heterolytic activation of H<sub>2</sub> and thus hydrogenation catalysis. The defect-rich Al<sub>2</sub>O<sub>3</sub> was prepared by simple calcination of a carboxylate-containing Al precursor. Combinatorial studies confirmed the presence of rich FLPs on the surface of the defective Al<sub>2</sub>O<sub>3</sub>. In contrast to conventional alumina (γ-Al<sub>2</sub>O<sub>3</sub>), the FLP-containing Al<sub>2</sub>O<sub>3</sub> can activate H<sub>2</sub> in the absence of any transition metal species. More importantly, H<sub>2</sub> was activated by surface FLPs in a heterolytic pathway, leading to the hydrogenation of styrene in a stepwise process. This work paves the way for the exploration of more underlying heterogeneous FLPs catalysts and further understanding of accurate active sites and catalytic mechanisms of heterogeneous FLPs at the molecular level.

Received 30th November 2023

Accepted 9th January 2024

DOI: 10.1039/d3sc06425e

rsc.li/chemical-science

## 1 Introduction

In catalytic hydrogenation of both chemical transformations and biological functions, most of the hydrogen (H<sub>2</sub>) activation processes occurred at the transition metal center.<sup>1–7</sup> The exploration of metal-free systems for H<sub>2</sub> activation is quite appealing while rather challenging.<sup>8</sup> Until 2006, Stephan and co-workers first reported one such unique system, the metal-free zwitterionic phosphoniumborate, which could reversibly activate H<sub>2</sub> under mild conditions. The proposed activation center of hydrogen was frustrated Lewis acid–base pairs (FLPs), which were defined as Lewis acids and bases sterically prevented from interaction to form Lewis acid–base adducts.<sup>9</sup> Since then, the traditional paradigm of Lewis acid–base chemistry was changed and development of new FLPs for promoting

chemical reactivity was heatedly pursued.<sup>10–13</sup> During the past few decades, a large number of homogeneous FLPs catalysts have been synthesized, which have found wide application in the fields of hydrogenation catalysis, small-molecule activation, organic chemistry, radical chemistry, transition metal chemistry, and enzyme models, as well as polymers and materials.<sup>14–16</sup>

Despite the significant progress, the studies on heterogeneous (semi-solid and solid) FLPs catalysts were rather limited.<sup>17–30</sup> The prominent examples included semi-solid (two-phase) FLPs catalysts of imine or nitrile modified gold nanoparticles,<sup>18</sup> as well as solid FLPs catalysts that covered atypical oxides such as In<sub>2</sub>O<sub>3–x</sub>(OH)<sub>y</sub> and CeO<sub>2–x</sub>.<sup>22,31</sup> The abundant homogeneous while rare heterogeneous FLP catalysts indicated the difficulty in the design and preparation of heterogeneous FLP catalysts, which was attributed to the poor understanding of the structure–property relationship of solid FLPs. As such, the development of simple and practical synthetic strategies, detailed characterization of active sites, and insight into the reaction mechanism of heterogeneous FLPs are of high importance.

Among oxide supports used in industry, alumina is generally considered to be inert to H<sub>2</sub> and thus make no contribution to the hydrogenation process by supported metal catalysts. Close examination of the literature revealed that, however, alumina after dehydration treatment at 450–650 °C was able to hydrogenate ethylene, in which the active sites were believed to chemisorb and polymerize olefins on alumina.<sup>32,33</sup> Nevertheless,

<sup>a</sup>New Cornerstone Science Laboratory, State Key Laboratory for Physical Chemistry of Solid Surfaces, Collaborative Innovation Center of Chemistry for Energy Materials, National & Local Joint Engineering Research Center of Preparation Technology of Nanomaterials, College of Chemistry and Chemical Engineering, Xiamen University, Xiamen 361005, China. E-mail: nzheng@xmu.edu.cn; xdyi@xmu.edu.cn

<sup>b</sup>Innovation Laboratory for Sciences and Technologies of Energy Materials of Fujian Province (IKKEM), Xiamen 361102, China

<sup>c</sup>Fujian Key Laboratory of Rare-Earth Functional Materials, Fujian Shanhai Collaborative Innovation Center of Rare-Earth Functional Materials, Longyan 366300, China

† Electronic supplementary information (ESI) available: Reagents, FTIR, TPD-MS, BET, XRD, HAADF-STEM, NMR, Fig. S1–S14 and Table S1. See DOI: <https://doi.org/10.1039/d3sc06425e>

‡ These authors contributed equally.



it remained elusive for the true active sites and the mechanism of the hydrogenation process.

Herein, we report the simple synthesis of a new type of pentacoordinated  $\text{Al}^{3+}$ -enriched  $\text{Al}_2\text{O}_3$ , in which a large number of Lewis acidic and basic sites are co-present on the surface. The rigidity of the solid lattice prevents them from interacting to be acid–base adducts, thus giving access to heterogeneous FLPs catalysts. Interestingly, the as-obtained  $\text{Al}_2\text{O}_3$  catalyst can activate hydrogen in the heterolytic pathway to produce equal amounts of  $\text{O-H}^{\delta+}$  and  $\text{Al-H}^{\delta-}$  in the absence of transition metals. The heterogeneous FLPs exhibited nice catalytic activity toward styrene hydrogenation in a stepwise mechanism.

## 2 Results and discussion

### 2.1 Preparation and characterization of the pentacoordinated $\text{Al}^{3+}$ -enriched $\text{Al}_2\text{O}_3$ catalyst

The pentacoordinated  $\text{Al}^{3+}$ -enriched defective  $\text{Al}_2\text{O}_3$  (denoted as d- $\text{Al}_2\text{O}_3$ ) catalyst was prepared by calcining aluminum hydroxide acetate,  $[\text{Al}(\text{OH})(\text{CH}_3\text{COO})_2]$ , at 500 °C in an inert atmosphere ( $\text{N}_2$  or Ar). The catalyst was first characterized by solid state  $^{27}\text{Al}$  magic-angle spinning nuclear magnetic resonance ( $^{27}\text{Al}$  MAS-NMR) spectroscopy (Fig. 1a).<sup>34</sup> Three peaks at chemical shifts of  $\sim 64$ , 33 and 6 ppm were assigned to  $\text{Al}^{3+}$  in tetrahedral ( $\text{Al}_t$ ), pentahedral ( $\text{Al}_p$ ) and octahedral ( $\text{Al}_o$ ) coordination environments, respectively. Unexpectedly, a large proportion of  $\text{Al}_p$  was observed in the as-prepared d- $\text{Al}_2\text{O}_3$ ,<sup>35</sup> while only  $\text{Al}_t$  and  $\text{Al}_o$  were present in the lattice of commercial  $\gamma$ - $\text{Al}_2\text{O}_3$  (Fig. 1a).<sup>36</sup> As surface atoms play a key role in both substrate interaction and chemical transformation, we then

compared the relative content of surface  $\text{Al}_p$  by using gaseous Lewis base molecules of  $\text{NH}_3$ .<sup>37–40</sup> As shown in Fig. 1b, the coordination of  $\text{NH}_3$  to surface  $\text{Al}_p$  led to a decrease in the intensity of the peak at  $\sim 33$  ppm and correspondingly a distinct increase of the peak at  $\sim 6$  ppm, suggesting the conversion of  $\text{Al}_p$  to  $\text{Al}_o$  after the treatment and thus the presence of rich Lewis acidic sites ( $\text{Al}_p$ ) on the surface of d- $\text{Al}_2\text{O}_3$ .<sup>36</sup> The content of  $\text{Al}_p$  decreased from 39.1% in d- $\text{Al}_2\text{O}_3$  to 23.8% in  $\text{NH}_3$ -d- $\text{Al}_2\text{O}_3$  (Fig. S1 and Table S1†). Thus, the portion of surface  $\text{Al}_p$  was estimated to be approximately 15.3% of the total  $\text{Al}^{3+}$  sites. The presence of surface  $\text{Al}_p$  on d- $\text{Al}_2\text{O}_3$  was also confirmed by *in situ* Fourier transform infrared spectroscopy of adsorbed  $\text{NH}_3$  (*in situ*  $\text{NH}_3$ -FTIR) and temperature-programmed desorption coupled with mass spectrometry using  $\text{NH}_3$  ( $\text{NH}_3$ -TPD-MS) (Fig. S2†). We also revealed that the d- $\text{Al}_2\text{O}_3$  surface featured richer and stronger Lewis basic sites than that of  $\gamma$ - $\text{Al}_2\text{O}_3$  by *in situ*  $\text{CO}_2$ -FTIR and  $\text{CO}_2$ -TPD-MS (Fig. S3†), although the specific surface area of  $\gamma$ - $\text{Al}_2\text{O}_3$  ( $176 \text{ m}^2 \text{ g}^{-1}$ ) was higher than that of d- $\text{Al}_2\text{O}_3$  ( $78 \text{ m}^2 \text{ g}^{-1}$ ) based on  $\text{N}_2$  adsorption/desorption isotherms (Fig. S4†). With the  $\text{Al}_p$  sites serving as the Lewis acid sites and the surface oxygen species acting as the Lewis base sites, the rigid structure of d- $\text{Al}_2\text{O}_3$  prevented them from interacting to form acid–base adducts, so obtained d- $\text{Al}_2\text{O}_3$  was rich in FLPs. In addition, X-ray powder diffraction (XRD) characterization revealed that in comparison to well-crystallized  $\gamma$ - $\text{Al}_2\text{O}_3$ , d- $\text{Al}_2\text{O}_3$  was much less crystallized, indicating that  $\text{Al}^{3+}$  ions in the alumina lattice of d- $\text{Al}_2\text{O}_3$  were highly disordered and in diverse coordination modes (Fig. S5†).<sup>35,41</sup> Aberration-corrected high-angle annular dark-field scanning transmission electron microscopy (HAADF-STEM) and fast Fourier transform (FFT) measurement also confirmed the amorphous characteristic of d- $\text{Al}_2\text{O}_3$  (Fig. S6†). These results match well with those of the solid state  $^{27}\text{Al}$  MAS-NMR.

### 2.2 FLPs as active sites for the catalytic hydrogenation of styrene

With the presence of a large amount of FLPs on the as-obtained d- $\text{Al}_2\text{O}_3$ , we then employed the hydrogenation of styrene as a model reaction to demonstrate the surface reactivity of d- $\text{Al}_2\text{O}_3$ . 50 mg catalyst of d- $\text{Al}_2\text{O}_3$  and 20  $\mu\text{L}$  styrene were added to 5 mL anhydrous toluene within a well-stirred autoclave, which was then charged with  $\text{H}_2$  to 1 MPa and kept at 100 °C. As shown in Fig. 1c, d- $\text{Al}_2\text{O}_3$  exhibited nice reactivity toward hydrogenation, as  $\sim 100\%$  styrene conversion was achieved within 4 h, and the complete conversion was confirmed using  $^1\text{H}$  NMR spectra (Fig. S7†). Moreover, recycling tests revealed that the d- $\text{Al}_2\text{O}_3$  catalyst did not deactivate after 8 cycles, suggesting high robustness of FLP structures on the d- $\text{Al}_2\text{O}_3$  surface (Fig. S8†). We noted that the presence of FLPs on d- $\text{Al}_2\text{O}_3$  was the key to achieving the catalytic activity. In the control experiment where no catalyst was used or  $\gamma$ - $\text{Al}_2\text{O}_3$  without surface FLPs was employed, no reactivity was observed (Fig. 1d). In addition, we also used a gaseous probe to validate the necessity of FLPs for the hydrogenation. When  $\text{NH}_3$  or  $\text{CO}_2$  was used to neutralize surface  $\text{Al}_p$  or basic sites, the catalytic activity of the d- $\text{Al}_2\text{O}_3$  was significantly declined (Fig. 1d). Based on the above

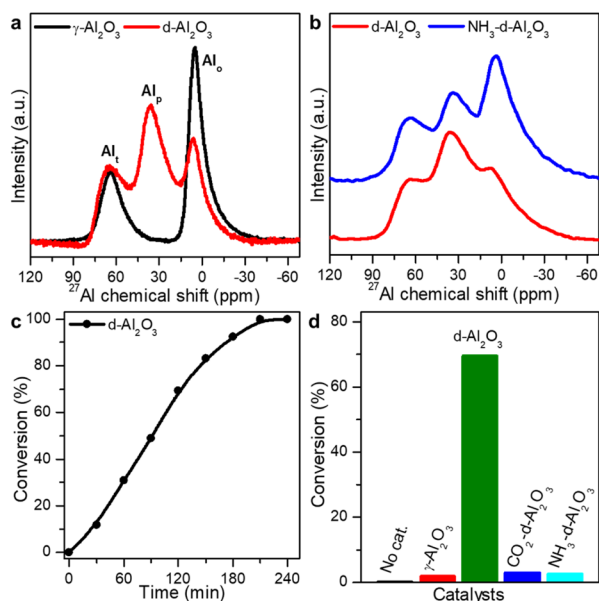


**Fig. 1** (a) Solid state  $^{27}\text{Al}$  MAS-NMR spectra of  $\gamma$ - $\text{Al}_2\text{O}_3$  and d- $\text{Al}_2\text{O}_3$ . (b) Solid state  $^{27}\text{Al}$  MAS-NMR spectra of d- $\text{Al}_2\text{O}_3$  and  $\text{NH}_3$  treated d- $\text{Al}_2\text{O}_3$ . (c) Catalytic hydrogenation of styrene by d- $\text{Al}_2\text{O}_3$ . (d) Catalytic performance comparison of no catalyst,  $\gamma$ - $\text{Al}_2\text{O}_3$ , d- $\text{Al}_2\text{O}_3$  and d- $\text{Al}_2\text{O}_3$ -treated with gaseous Lewis acid or base molecules of  $\text{CO}_2$  and  $\text{NH}_3$ , respectively. Reaction time: 120 min.



observations, we considered that FLPs were the real active centers for the catalytic hydrogenation of styrene.

### 2.3 Heterolytic activation of H<sub>2</sub> on FLPs on d-Al<sub>2</sub>O<sub>3</sub>

The unexpected hydrogenation activity motivated us to deeply understand the H<sub>2</sub> activation and hydrogenation mechanism over the heterogeneous FLPs. The feature of activated hydrogen species on the solid product was first characterized directly by two-dimensional (2D) solid state heteronuclear correlation (HETCOR) NMR spectroscopy.<sup>42,43</sup> Compared to H<sub>2</sub>-treated  $\gamma$ -Al<sub>2</sub>O<sub>3</sub>, we detected an additionally intense cross peak linking the Al<sub>p</sub> site and H <sup>$\delta^-$</sup>  products in H<sub>2</sub>-treated d-Al<sub>2</sub>O<sub>3</sub> with a short CP contact time (Fig. 2a and S9<sup>†</sup>). This suggests that H species are adjacent to Al<sub>p</sub> sites.<sup>44</sup> Additionally, we confirmed the existence of Al<sub>p</sub>-bonded hydrogen species (Al<sub>p</sub>-H <sup>$\delta^-$</sup> ) through *in situ* H<sub>2</sub>-FTIR spectroscopy. An obvious peak in the range of 1730–1970 cm<sup>-1</sup> confirmed the presence of Al<sub>p</sub>-H <sup>$\delta^-$</sup>  in H<sub>2</sub>-treated d-Al<sub>2</sub>O<sub>3</sub>, and abundant O-H <sup>$\delta^+$</sup>  species were observed on the surface of H<sub>2</sub>-treated d-Al<sub>2</sub>O<sub>3</sub> (Fig. 2b). The above results convincingly revealed that H<sub>2</sub> was activated at the FLP sites *via* the heterolytic activation pathway with the formation of Al<sub>p</sub>-H <sup>$\delta^-$</sup>  and O-H <sup>$\delta^+$</sup> .<sup>45–48</sup> Furthermore, considering the complicated chemical environment of hydrogen species in the sample,<sup>49,50</sup> some bound to FLPs while others not, we employed <sup>2</sup>H to probe the hydrogen species on the FLPs to exclude other influencing factors.<sup>51</sup> As shown in Fig. 2c (red trace), the solid state <sup>2</sup>H MAS-NMR spectra of D<sub>2</sub>-treated d-Al<sub>2</sub>O<sub>3</sub> showed a peak at 4.2 ppm corresponding to the <sup>2</sup>H NMR signal of D<sub>2</sub>O (Fig. S10<sup>†</sup>),<sup>52</sup> which represented the activated hydrogen species on the FLPs. In contrast to d-Al<sub>2</sub>O<sub>3</sub>, no <sup>2</sup>H signal was detected when  $\gamma$ -Al<sub>2</sub>O<sub>3</sub> was

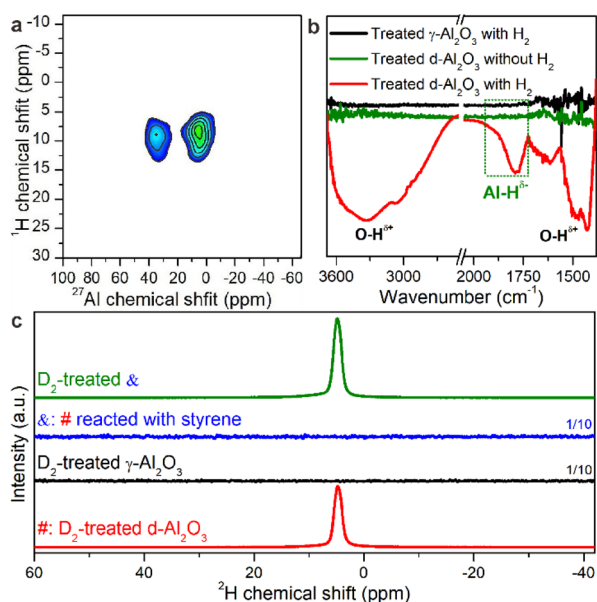


Fig. 2 (a) 2D solid state <sup>1</sup>H–<sup>27</sup>Al HETCOR spectrum of H<sub>2</sub>-treated d-Al<sub>2</sub>O<sub>3</sub>. (b) *In situ* H<sub>2</sub>-FTIR of  $\gamma$ -Al<sub>2</sub>O<sub>3</sub>, d-Al<sub>2</sub>O<sub>3</sub> treated without H<sub>2</sub> and d-Al<sub>2</sub>O<sub>3</sub> treated with H<sub>2</sub>. (c) Solid state <sup>2</sup>H MAS-NMR spectra of D<sub>2</sub>-treated d-Al<sub>2</sub>O<sub>3</sub> (denoted as #), D<sub>2</sub>-treated  $\gamma$ -Al<sub>2</sub>O<sub>3</sub>, # reacted with styrene (denoted as θ), and D<sub>2</sub>-treated θ.

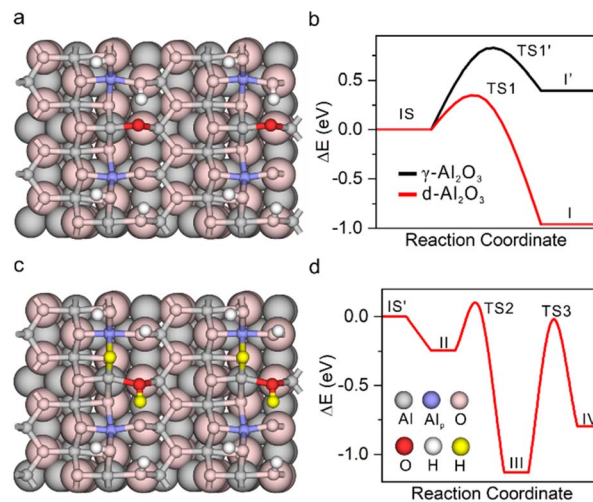


Fig. 3 Structure of (a) d-Al<sub>2</sub>O<sub>3</sub> and (c) d-Al<sub>2</sub>O<sub>3</sub> with heterolytically dissociated H<sub>2</sub>. The colour code is shown in panel (d). Energetic profiles of (b) H<sub>2</sub> activation over  $\gamma$ -Al<sub>2</sub>O<sub>3</sub> and d-Al<sub>2</sub>O<sub>3</sub>, and (d) following stepwise hydrogenation of C<sub>2</sub>H<sub>4</sub> over d-Al<sub>2</sub>O<sub>3</sub>.

treated with D<sub>2</sub> under the same conditions (Fig. 3c, black trace). These results clearly indicate that d-Al<sub>2</sub>O<sub>3</sub> with FLPs readily activates H<sub>2</sub>, while  $\gamma$ -Al<sub>2</sub>O<sub>3</sub> without FLPs did not. Moreover, *in situ* D<sub>2</sub>-FTIR spectroscopy demonstrated that d-Al<sub>2</sub>O<sub>3</sub> activated D<sub>2</sub> rather than  $\gamma$ -Al<sub>2</sub>O<sub>3</sub>, as indicated by the distinct signal of the O–D bond during the treatment of d-Al<sub>2</sub>O<sub>3</sub> with D<sub>2</sub> (Fig. S11<sup>†</sup>). The activated hydrogen species (O–H <sup>$\delta^+$</sup>  and Al–H <sup>$\delta^-$</sup> ) formed on the FLPs of d-Al<sub>2</sub>O<sub>3</sub> reacted readily with styrene. As shown by solid state <sup>2</sup>H MAS-NMR, the <sup>2</sup>H signal of the deuterated species from the d-Al<sub>2</sub>O<sub>3</sub> treated with D<sub>2</sub> disappeared upon the introduction of styrene (Fig. 2c, blue trace). When the d-Al<sub>2</sub>O<sub>3</sub> catalyst was treated with D<sub>2</sub> again after the reaction with styrene, the <sup>2</sup>H signal reappeared (Fig. 2c, green trace).

DFT calculation was further applied to understand the hydrogenation process.<sup>53–55</sup> The structure of  $\gamma$ -Al<sub>2</sub>O<sub>3</sub> was constructed following the same method in our previous study.<sup>56</sup> The d-Al<sub>2</sub>O<sub>3</sub> model with surface Al<sub>p</sub> was constructed from  $\gamma$ -Al<sub>2</sub>O<sub>3</sub> following a dehydration process. Considering the high surface concentration of Al<sub>p</sub> on the surface of d-Al<sub>2</sub>O<sub>3</sub> reported in this work, 1/2 surface hydroxyl group was removed. The resulting coordinatively unsaturated Al<sub>p</sub> site and the deprotonated –O– site serve as the FLP center for the H<sub>2</sub> activation and hydrogenation (Fig. 3a). By overcoming a barrier of 0.30 eV (TS1), the heterolytic dissociation of H<sub>2</sub> at the FLP site was exothermic by ~0.96 eV over d-Al<sub>2</sub>O<sub>3</sub> (Fig. 3b), resulting in O–H <sup>$\delta^+$</sup>  and Al<sub>p</sub>-H <sup>$\delta^-$</sup>  (Fig. 3c). By contrast, the dissociation of H<sub>2</sub> on  $\gamma$ -Al<sub>2</sub>O<sub>3</sub> can be only realized on the surface with reconstruction of the surface Al<sub>t</sub> with a barrier of 0.82 eV (TS1') and endothermicity of 0.40 eV (Fig. S12<sup>†</sup>), implying that the activation of H<sub>2</sub> on the pristine  $\gamma$ -Al<sub>2</sub>O<sub>3</sub> was restricted. The hydrogenation of ethylene was further calculated to confirm that the heterolytically dissociated hydrogen species were responsible for the catalytic hydrogenation. As shown in Fig. 3d and S13<sup>†</sup>, the barriers for the stepwise hydride and proton transfer from Al<sub>p</sub>-H <sup>$\delta^-$</sup>  and O–H <sup>$\delta^+$</sup>  to



produce ethane were 0.31 (TS2) and 1.11 eV (TS3), respectively, which was affordable under the catalytic conditions.

## 2.4 Stepwise hydrogenation mechanism

The catalytic hydrogenation mechanism utilizing  $\text{O-H}^{\delta+}$  and  $\text{Al-H}^{\delta-}$  species on FLPs was also verified by isotope-labelling experiments. First, when  $\text{D}_2$ -treated  $\text{d-Al}_2\text{O}_3$  was used to react with styrene in anhydrous toluene, the characteristic peaks of deuterated ethylbenzene were observed in  $^2\text{H}$  NMR spectra (Fig. 4a), indicating that the  $\text{D}_2$  dissociated on FLPs of  $\text{d-Al}_2\text{O}_3$  can deuterate styrene and thus verifying the results observed in Fig. 2c. Correspondingly, when  $\text{D}_2$  was used as the hydrogen source and  $\text{D}_2$  treated  $\text{d-Al}_2\text{O}_3$  as the catalyst, a very strong signal of deuterated ethylbenzene without the presence of other impurities was observed in the  $^2\text{H}$  NMR spectrum, further confirming that  $\text{d-Al}_2\text{O}_3$  can catalyze hydrogenation of styrene to afford ethylbenzene in  $\sim 100\%$  purity (Fig. 4b). Interestingly, we found that the number of D atoms on the alpha carbon atom ( $\text{C}_\alpha$ ) was significantly less than that on the beta carbon atom ( $\text{C}_\beta$ ). The peak area ratio,  $\alpha_{\text{D}}:\beta_{\text{D}}$ , was calculated to be 1:2.6 (Fig. 4c). The results suggested the existence of the hydrogen–deuterium exchange in the hydrogenation process, which was an indication that the hydrogenation reaction was performed in two steps rather than one step.<sup>57</sup> As expected, when  $\text{D}_2$  and  $\text{H}_2$  were used as hydrogen sources respectively, a typical primary kinetic isotope effect (KIE,  $k_{\text{H}_2}/k_{\text{D}_2} > 5$ ) was observed (Fig. 4d), so the rate-determining step was the cleavage of the O–D bond.<sup>58,59</sup>

Based on the above systematic studies, the catalytic pathway of the reaction was proposed (Fig. S14<sup>†</sup>). The reaction begins with the heterolytic activation of  $\text{H}_2$  by FLPs of  $\text{d-Al}_2\text{O}_3$  to produce  $\text{O-H}^{\delta+}$  and  $\text{Al-H}^{\delta-}$ . Next, the active hydride species react with the adsorbed styrene following an Eley–Rideal-like mechanism, attacking  $\beta_{\text{C}}$ , and then the protons at the O atom interact with  $\alpha_{\text{C}}$ . Finally, the obtained ethylbenzene was released and the catalytically active sites were recovered.

## 2.5 $\text{d-Al}_2\text{O}_3$ as the catalyst for hydrogenation of other substrates

Furthermore, insight into the mechanism also motivated us to explore the general applicability of the  $\text{d-Al}_2\text{O}_3$  catalyst. Table 1 shows the results of these hydrogenation reactions. First,  $\text{d-Al}_2\text{O}_3$  exhibited nice activity in the hydrogenation of various olefins including aromatic and aliphatic olefins (Table 1, entries 1–4). Moreover, the hydrogenation of aromatic and aliphatic alkynes over  $\text{d-Al}_2\text{O}_3$  gave the corresponding alkanes with excellent yields too (Table 1, entries 5–9). These results strongly suggested that FLPs enabled the

Table 1 Hydrogenation of olefins, alkanes, benzaldehyde and acetophenone catalysed by the  $\text{d-Al}_2\text{O}_3$  catalyst<sup>a</sup>

Entry	Substrate	Product	Yield (%)
1 <sup>b</sup>			>99.5
2 <sup>b</sup>			>99.0
3 <sup>b</sup>			>99.9
4 <sup>b</sup>			>99.9
5 <sup>b</sup>			>99.5
6 <sup>b</sup>			>98.5
7 <sup>b</sup>			>99.9
8 <sup>b</sup>			>99.0
9 <sup>b</sup>			>99.5
10 <sup>c</sup>			>98.5
11 <sup>c</sup>			>99.0

<sup>a</sup> Reaction conditions: 50 mg  $\text{d-Al}_2\text{O}_3$ , 0.2 mmol substrate, 5 mL anhydrous toluene. <sup>b</sup> 100 °C, 8 h, 1 MPa  $\text{H}_2$ . <sup>c</sup> 150 °C, 24 h, 4 MPa  $\text{H}_2$ .

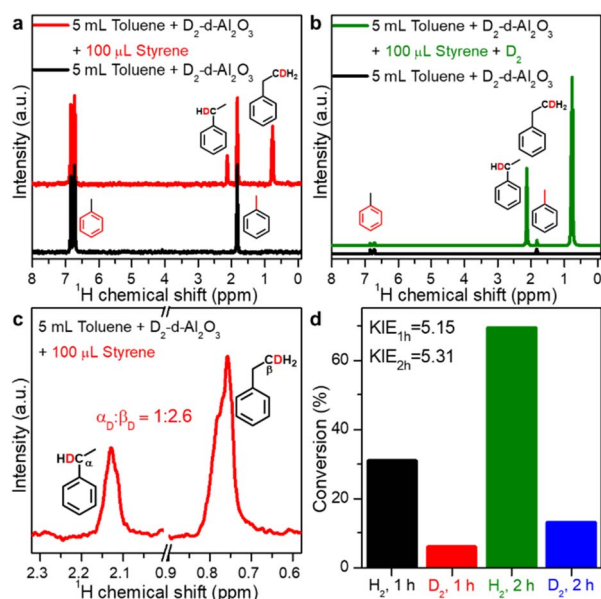


Fig. 4 (a)  $^2\text{H}$  NMR spectra of toluene mixed with  $\text{D}_2$ -treated  $\text{d-Al}_2\text{O}_3$  and  $\text{d}$ -ethylbenzene from reacting styrene with  $\text{D}_2$ -treated  $\text{d-Al}_2\text{O}_3$  in toluene. (b)  $^2\text{H}$  NMR spectra of toluene mixed with  $\text{D}_2$ -treated  $\text{d-Al}_2\text{O}_3$  and  $\text{d}$ -ethylbenzene from reacting styrene with  $\text{D}_2$  and  $\text{D}_2$ -treated  $\text{d-Al}_2\text{O}_3$  in toluene. (c) Enlargement of the two peaks of  $\alpha_{\text{D}}$  and  $\beta_{\text{D}}$  in Fig. 4a. (d) Primary kinetic isotope effect (PKIE) of styrene hydrogenation.



hydrogenation of both terminal and internal carbon-carbon multiple bonds. Since heterolytic activation of H<sub>2</sub> yielded both O-H<sup>δ+</sup> and Al-H<sup>δ-</sup> on the d-Al<sub>2</sub>O<sub>3</sub> surface, d-Al<sub>2</sub>O<sub>3</sub> should allow the hydrogenation of polar unsaturated bonds.<sup>60-62</sup> As expected, we observed good catalytic performance in the hydrogenation of benzaldehyde or acetophenone by d-Al<sub>2</sub>O<sub>3</sub> (Table 1, entries 10-11).

### 3 Conclusions

In summary, amorphous Al<sub>2</sub>O<sub>3</sub> enriched with surface penta-coordinated Al<sup>3+</sup> species has been synthesized *via* a simple synthesis method. The co-presence of a large amount of Lewis acidic and basic sites in the same rigid phase thus gave rise to a new type of heterogeneous transition metal-free FLP catalyst. The d-Al<sub>2</sub>O<sub>3</sub> catalyst is highly reactive to enable the heterolytic activation of molecular hydrogen. In the hydrogenation of styrene, the FLP-enriched d-Al<sub>2</sub>O<sub>3</sub> exhibited nice activity and robustness, and more importantly, a stepwise hydrogenation mechanism. Since heterolytic activation of H<sub>2</sub> yielded both O-H<sup>δ+</sup> and Al-H<sup>δ-</sup> on the d-Al<sub>2</sub>O<sub>3</sub> surface, d-Al<sub>2</sub>O<sub>3</sub> catalyzed the hydrogenation of polar unsaturated bonds in aldehydes or ketones. More work on employing FLP-rich oxides for the discovery of other exciting catalysts should be further explored.

### 4 Experimental methods

#### 4.1 General procedure for synthesis of d-Al<sub>2</sub>O<sub>3</sub>

For a typical synthesis process of d-Al<sub>2</sub>O<sub>3</sub>, 500 mg Al(OH)(CH<sub>3</sub>-COO)<sub>2</sub> was transferred into a glass reaction tube (Φ = 1 cm). The sample was heated to 500 °C at a rate of temperature increase of 1 °C min<sup>-1</sup> for 4 h under N<sub>2</sub> or Ar protection. After cooling to room temperature, the white products were quickly transferred to a dry centrifuge tube, sealed and stored in a desiccator, and used for further characterization.

#### 4.2 General procedure for treatment of d-Al<sub>2</sub>O<sub>3</sub> with gaseous Lewis base molecules

For a typical treatment process, d-Al<sub>2</sub>O<sub>3</sub> was first synthesized by the above method in a glass reaction tube. After cooling to room temperature, high-purity gases (5 vol% NH<sub>3</sub>/Ar) at a rate of 20 mL min<sup>-1</sup> were passed with mass flow for 12 h. The products were quickly transferred to a dry centrifuge tube, sealed and stored in a desiccator, as well as used for further characterization. The samples were marked as NH<sub>3</sub>-d-Al<sub>2</sub>O<sub>3</sub>.

#### 4.3 General procedure for treatment of d-Al<sub>2</sub>O<sub>3</sub> with H<sub>2</sub> or D<sub>2</sub>

For a typical treatment process, d-Al<sub>2</sub>O<sub>3</sub> was first synthesized by the above method in a glass reaction tube. After cooling to room temperature, the sample was heated to 100 °C at a rate of temperature increase of 1 °C min<sup>-1</sup> for 2 h under H<sub>2</sub> or D<sub>2</sub> protection. After cooling to room temperature, the products were quickly transferred to a dry centrifuge tube, sealed and stored in a desiccator, which was used for further characterization and applications.

#### 4.4 General procedure for catalysis tests

For a typical styrene hydrogenation reaction, a freshly prepared 50 mg catalyst of d-Al<sub>2</sub>O<sub>3</sub> was dispersed in 5 mL anhydrous toluene, and then 20 μL styrene was added in an autoclave under stirring. Next, the reactor was charged with H<sub>2</sub> to 1 MPa and kept at 100 °C in an oil bath during stirring. The products were analyzed by gas chromatography (GC9720Plus, Fuli Instruments) for conversion determination. For other catalysts, the reaction conditions were the same as above. In the catalyst recycling test, after the first cycle was carried out for 150 min, the same amount of styrene was added to the reactor and the reaction was allowed to take place. As mentioned above, the recycling was repeated another six times.

#### 4.5 Solid state <sup>27</sup>Al MAS NMR characterization

Solid state <sup>27</sup>Al MAS-NMR measurement (Fig. 1a) was performed using a Bruker Avance NEO 600 MHz spectrometer with a 3.2 mm probe head at a spinning rate of 20 kHz. Spectra were accumulated for 1000 scans with a cycle delay of 2.5 s, using a pulse width of π/6. Solid state <sup>27</sup>Al MAS-NMR measurement (Fig. 1b) was performed using a Bruker Avance III 400 MHz spectrometer with a 4.0 mm probe head at a spinning rate of 12 kHz. Spectra were accumulated for 256 scans with a recycle delay of 2 s and a pulse width of π/2 was used. It is worth noting that the magnetic field strength and pulse width hardly affected the relative content of Al<sup>3+</sup> ions in the different coordination environments in our test. The fitting of <sup>27</sup>Al NMR spectra was conducted using the Dmfit program, which includes the quadrupolar interactions for <sup>27</sup>Al MAS NMR. The Czsimple model was applied for the fitting, which implements a rapid version of the Cjzjek distribution of quadrupolar interaction. The Gaussian isotropic model for *d* = 5 with an uncoupled distribution of isotropic chemical shift was included in the simulations. All the other parameters were freely variable during the fitting.<sup>63</sup>

#### 4.6 2D solid state <sup>1</sup>H-<sup>27</sup>Al heteronuclear correlation (HETCOR) experiment

The experiment was performed on a Bruker Avance NEO 600 MHz spectrometer with a 3.2 mm probe head under MAS conditions of 15 kHz with a very short CP contact time of 50 μs.

#### 4.7 Solid state <sup>2</sup>H MAS NMR characterization

Solid state <sup>2</sup>H MAS NMR spectra were recorded on a Bruker Avance III NEO 600 MHz spectrometer with a 3.2 mm probe head at a spinning rate of 15 kHz, and the spectra were accumulated for 1024 scans with a cycle delay of 1 s, and a pulse width of π/2 was used.

#### 4.8 Liquid state <sup>1</sup>H NMR characterization

<sup>1</sup>H NMR spectra were recorded on an AVANCE III 500 MHz spectrometer.



#### 4.9 Liquid state $^2\text{H}$ NMR characterization

$^2\text{H}$  NMR spectra were recorded on an AVANCE III 850 MHz spectrometer. All NMR data were processed on MestReNova software.

#### 4.10 *In situ* diffuse reflectance FTIR characterization

Typically,  $\text{d-Al}_2\text{O}_3$  was first synthesized in an *in situ* chamber of FTIR (Thermo Fisher IS50) at 500 °C under Ar protection, and the sample was cooled to 30 °C to acquire background. For *in situ*  $\text{NH}_3$ -FTIR, 5 vol%  $\text{NH}_3/\text{Ar}$  was charged into the chamber at a rate of 30 mL  $\text{min}^{-1}$  while pure Ar was turned off, and spectra were collected until stable adsorption with  $\text{NH}_3$ . *In situ*  $\text{CO}_2$ -FTIR spectra were recorded in the same way. *In situ*  $\text{D}_2$ -FTIR spectra were recorded in the same way except that the test temperature is 100 °C.

#### 4.11 TPD-MS characterization

Typically,  $\text{NH}_3$ -TPD-MS was performed on a Micromeritics AutoChem II 2920 instrument equipped with a mass spectrometer. The 100 mg  $\text{d-Al}_2\text{O}_3$  sample was first synthesized at 500 °C under Ar protection. The sample was then cooled to room temperature and treated under 5 vol%  $\text{NH}_3/\text{He}$  gas flow for 30 min. The gaseous and weakly adsorbed  $\text{NH}_3$  was subsequently removed by purging with He for 60 min. Subsequently, the temperature was raised from room temperature to 700 °C at a rate of 10 °C  $\text{min}^{-1}$  and the  $\text{NH}_3$ -TPD profile was recorded by using a mass spectrometer with a signal of  $m/z = 16$ . For  $\text{CO}_2$ -TPD-MS, 5 vol%  $\text{CO}_2/\text{He}$  gas was used, and the  $\text{CO}_2$ -TPD profile was recorded by using a mass spectrometer with a signal of  $m/z = 44$ .

#### 4.12 $\text{N}_2$ adsorption/desorption characterization

$\text{N}_2$  adsorption/desorption measurements were conducted on a Micromeritics ASAP 2020 gas adsorption analyzer. The freshly prepared sample was first degassed at 300 °C for 8 h. Then, the specific surface areas were determined using the Brunauer–Emmett–Teller (BET) and Langmuir equations from the  $\text{N}_2$  sorption data.

#### 4.13 XRD characterization

X-ray powder diffraction experiments were conducted on a Rigaku Ultima IV using  $\text{Cu K}\alpha$  radiation. The operation voltage and current were 40 kV and 30 mA, respectively. The scanning speed was set to be 15 °  $\text{min}^{-1}$ .

#### 4.14 HAADF-STEM characterization

High-angle annular-dark-field (HAADF) images were acquired using a JEOL 200F transmission electron microscope operated at 200 keV. The attainable spatial resolution of the microscope was 78 pm with a probe spherical-aberration corrector. Images were acquired with the illumination semi-angle of 25 mrad and probe current of 100 pA. The dwell time for image acquisition was set at 10 microseconds per pixel to ensure a desirable signal-to-noise ratio.

#### 4.15 Computational details

The spin-polarized density functional theory (DFT) calculations were performed using the Vienna *ab initio* simulation package (VASP5.4.4).<sup>64–67</sup> The core electrons were replaced by the projector augmented wave (PAW) pseudopotentials,<sup>65,68</sup> and the valence electrons were described by a plane wave basis set with a cut-off energy of 400 eV. The electron exchange and correlation were treated by Perdew–Burke–Ernzerhof (PBE) generalized gradient approximation (GGA).<sup>69</sup> The  $k$ -point sampling was generated by following the Monkhorst–Pack procedure with a  $3 \times 3 \times 1$  mesh.<sup>70</sup> The transition states (TSs) were determined using the nudged elastic band (NEB) approach. The TS structures were optimized using a quasi-Newton algorithm. The steady states and TSs were converged to a residual force smaller than 0.03 eV  $\text{\AA}^{-1}$  and 0.05 eV  $\text{\AA}^{-1}$ , respectively. All the minima and TSs were confirmed by the vibrational frequency calculations. The reaction barrier was defined as  $\Delta E_a = E_{\text{TS}} - E_{\text{R}}$ , where  $E_{\text{R}}$  and  $E_{\text{TS}}$  were the energies of the reactant on the slab and the corresponding transition states, respectively.

### Data availability

All the data supporting this article have been included in ESI.†

### Author contributions

N. F. Z. conceived and supervised the research project. Q. Y. W. synthesized and characterized the samples, as well as investigated the catalytic performances and mechanism. R. X. Q. performed DFT calculations. M. S. Z., Y. Y. Z and S. S. Y. contributed to the NMR and TPD measurements. G. F. provided some suggestions. N. F. Z., and Q. Y. W. wrote and revised the manuscript. X. D. Y and H. S. revised the manuscript.

### Conflicts of interest

The authors declare no competing financial interests.

### Acknowledgements

We acknowledge financial support from the National Natural Science Foundation of China (grant no. 92261207, 22202164, and NSFC Center for Single-Atom Catalysis under grant no. 22388102) and the New Cornerstone Science Foundation. Q. Y. W. thanks the China Postdoctoral Science Foundation Project (2023M732946). R. X. Q. acknowledges support from National Key R&D Program of China (2022YFA1504500), the Natural Science Foundation of Fujian Province (2023J05006) and the Fundamental Research Funds for the Central Universities (20720230002). We also thank Prof. Lin Gu and Dr Qinghua Zhang at the Institute of Physics of the Chinese Academy of Sciences for the TEM measurements.

### References

- 1 G. S. McGrady and G. Guilera, *Chem. Soc. Rev.*, 2003, **32**, 383.
- 2 G. J. Kubas, *Acc. Chem. Res.*, 1988, **21**, 120.



- 3 D. M. Heinekey, A. Lledos and J. M. Lluch, *Chem. Soc. Rev.*, 2004, **33**, 175.
- 4 P. G. Jessop and R. H. Morris, *Coord. Chem. Rev.*, 1992, **121**, 155.
- 5 A. I. Krasna and D. Rittenberg, *J. Am. Chem. Soc.*, 1954, **76**, 3015.
- 6 D. Schilter, J. M. Camara, M. T. Huynh, S. S. Hammes and T. B. Rauchfuss, *Chem. Rev.*, 2016, **116**, 8693.
- 7 W. Lubitz, H. Ogata, O. Rudiger and E. Reijerse, *Chem. Rev.*, 2014, **114**, 4081.
- 8 S. Aldridge and A. J. Downs, *Chem. Rev.*, 2001, **101**, 3305.
- 9 G. C. Welch, R. R. San Juan, J. D. Masuda and D. W. Stephan, *Science*, 2006, **314**, 1124.
- 10 P. Spies, G. Erker, G. Kehr, K. Bergander, R. Frohlich, S. Grimme and D. W. Stephan, *Chem. Commun.*, 2007, 5072.
- 11 G. C. Welch and D. W. Stephan, *J. Am. Chem. Soc.*, 2007, **129**, 1880.
- 12 P. A. Chase, G. C. Welch, T. Jurca and D. W. Stephan, *Angew. Chem., Int. Ed.*, 2007, **119**, 8196.
- 13 G. C. Welch, L. Cabrera, P. A. Chase, E. Hollink, J. D. Masuda, P. Wei and D. W. Stephan, *Dalton Trans.*, 2007, 3407.
- 14 D. W. Stephan, *Science*, 2016, **354**, aaf7229.
- 15 D. W. Stephan and G. Erker, *Angew. Chem., Int. Ed.*, 2010, **49**, 46.
- 16 D. W. Stephan, *Acc. Chem. Res.*, 2015, **48**, 306.
- 17 Y. Ma, S. Zhang, C. Chang, Z. Huang, J. Ho and Y. Qu, *Chem. Soc. Rev.*, 2018, **47**, 5541.
- 18 G. Lu, P. Zhang, D. Sun, L. Wang, K. Zhou, Z. Wang and G. Guo, *Chem. Sci.*, 2014, **5**, 1082.
- 19 K. C. Szeto, W. Sahyoun, N. Merle, J. L. Castelbou, N. Popoff, F. Lefebvre, J. Raynaud, C. Godard, C. Claver, L. Delevoeye, R. M. Gauvin and M. Taoufik, *Catal. Sci. Technol.*, 2016, **6**, 882.
- 20 J. Y. Xing, J. C. Buffet, N. H. Rees, P. Norby and D. O'Hare, *Chem. Commun.*, 2016, **52**, 10478.
- 21 K. K. Ghuman, T. E. Wood, L. B. Hoch, C. A. Mims, G. A. Ozin and C. V. Singh, *Phys. Chem. Chem. Phys.*, 2015, **17**, 14623.
- 22 K. K. Ghuman, L. B. Hoch, P. Szymanski, J. Y. Y. Loh, N. P. Kherani, M. A. El-Sayed, G. A. Ozin and C. V. Singh, *J. Am. Chem. Soc.*, 2016, **138**, 1206.
- 23 L. He, T. E. Wood, B. Wu, Y. Dong, L. B. Hoch, L. M. Reyes, D. Wang, C. Kübel, C. Qian, J. Jia, K. Liao, P. G. O'Brien, A. Sandhel, J. Y. Y. Loh, P. Szymanski, N. P. Kherani, T. C. Sum, C. A. Mims and G. A. Ozin, *ACS Nano*, 2016, **10**, 5578.
- 24 L. B. Hoch, L. He, Q. Qiao, K. Liao, L. M. Reyes, Y. Zhu and G. A. Ozin, *Chem. Mater.*, 2016, **28**, 4160.
- 25 A. Primo, F. Neatu, M. Florea, V. Parvulescu and H. Garcia, *Nat. Commun.*, 2014, 5291.
- 26 J. Zhao, X. Liu and Z. Chen, *ACS Catal.*, 2017, **7**, 766.
- 27 X. Zhao, J. Wang, M. Yang, N. Lei, L. Li, B. Hou, S. Miao, X. Pan, A. Wang and T. Zhang, *ChemSusChem*, 2017, **10**, 819.
- 28 H. Lee, Y. N. Choi, D. W. Lim, M. M. Rahman, Y. I. Kim, I. H. Cho, H. W. Kang, J. H. Seo, C. Jeon and K. B. Yoon, *Angew. Chem., Int. Ed.*, 2015, **54**, 13080.
- 29 T. Mahdi and D. W. Stephan, *Angew. Chem., Int. Ed.*, 2015, **54**, 8511.
- 30 M. Trunk, J. F. Teichert and A. Thomas, *J. Am. Chem. Soc.*, 2017, **139**, 3615.
- 31 S. Zhang, Z. Huang, Y. Ma, W. Gao, J. Li, F. Cao, L. Li, C. Chang and Y. Qu, *Nat. Commun.*, 2017, **8**, 15266.
- 32 S. G. Hindin and S. W. Weller, *J. Phys. Chem.*, 1956, **60**, 1501.
- 33 Y. Amenomiya, J. H. B. Chenier and R. J. Cvetanovic, *J. Catal.*, 1967, **9**, 28.
- 34 J. H. Kwak, J. Hu, D. Mei, C. W. Yi, D. H. Kim, C. H. Peden, L. F. Allard and J. Szanyi, *Science*, 2009, **325**, 1670.
- 35 N. Tang, Y. Cong, Q. Shang, C. Wu, G. Xu and X. Wang, *ACS Catal.*, 2017, **7**, 5987.
- 36 Z. Zhang, Y. Zhu, H. Asakura, B. Zhang, J. Zhang, M. Zhou, Y. Han, T. Tanaka, A. Wang, T. Zhang and N. Yan, *Nat. Commun.*, 2017, **8**, 16100.
- 37 P. Liu, R. Qin, G. Fu and N. F. Zheng, *J. Am. Chem. Soc.*, 2017, **139**, 2122.
- 38 Q. Wu, R. Qin, D. Zang, W. Zhang, B. Wu and N. F. Zheng, *Acta Chim. Sin.*, 2018, **76**, 617.
- 39 R. Qin, K. Liu, Q. Wu and N. F. Zheng, *Chem. Rev.*, 2020, **120**, 11810.
- 40 Q. Wu, W. Zhou, H. Shen, R. Qin, Q. Hong, X. Yi and N. Zheng, *CCS Chem.*, 2023, **5**, 1215.
- 41 L. Shi, G. M. Deng, W. C. Li, S. Miao, Q. N. Wang, W. P. Zhang and A. H. Lu, *Angew. Chem., Int. Ed.*, 2015, **54**, 13994.
- 42 S. h. Xin, Q. Wang, J. Xu, N. D. Feng, W. Z. Li and F. Deng, *Solid State Nucl. Magn. Reson.*, 2017, **84**, 103.
- 43 L. Wang, G. Kehr, C. G. Daniliuc, M. Brinkkötter, T. Wiegand, A.-L. Wübker, H. Eckert, L. Liu, J. G. Brandenburg, S. Grimme and G. Erker, *Chem. Sci.*, 2018, **9**, 4859.
- 44 K. R. Graham, C. Cabanetos, J. P. Jahnke, M. N. Idso, A. El Labban, G. O. Ngongang Ndjawa, T. Heumueller, K. Vandewal, A. Salleo, B. F. Chmelka, A. Amassian, P. M. Beaujuge and M. D. McGehee, *J. Am. Chem. Soc.*, 2014, **136**, 9608.
- 45 B. Werghi, A. Bendjeriou-Sedjerari, A. Jedidi, E. Abou-Hamad, L. Cavallo and J. M. Basset, *Organometallics*, 2016, **35**, 3288.
- 46 M. Veith, J. Frères, V. Huch and M. Zimmer, *Organometallics*, 2006, **25**, 1875.
- 47 R. Wischert, C. Coperet, F. Delbecq and P. Sautet, *Angew. Chem., Int. Ed.*, 2011, **123**, 3260.
- 48 J. Joubert, A. Salameh, V. Krakoviack, F. Delbecq, P. Sautet, C. Copéret and J. M. Basset, *J. Phys. Chem. B*, 2006, **110**, 23944.
- 49 H. Shen, Q. Wu, M. S. Asre Hazer, X. Tang, Y.-Z. Han, R. Qin, C. Ma, S. Malola, B. K. Teo, H. Häkkinen and N. Zheng, *Chem*, 2022, **8**, 2380.
- 50 H. Shen, Q. Wu, S. Malola, Y.-Z. Han, Z. Xu, R. Qin, X. Tang, Y.-B. Chen, B. K. Teo, H. Häkkinen and N. Zheng, *J. Am. Chem. Soc.*, 2022, **144**, 10844.
- 51 C. Sun, N. Mammen, S. Kaappa, P. Yuan, G. Deng, C. Zhao, J. Yan, S. Malola, K. Honkala, H. Hakkinen, B. K. Teo and N. Zheng, *ACS Nano*, 2019, **13**, 5975.



- 52 T. Mizuno, T. Nemoto, M. Tansho, T. Shimizu, H. Ishii and K. Takegoshi, *J. Am. Chem. Soc.*, 2006, **128**, 9683.
- 53 W. Zhang, R. Qin, G. Fu and N. Zheng, *J. Am. Chem. Soc.*, 2023, **145**, 10178.
- 54 K. Li, R. Qin, K. Liu, W. Zhou, N. Liu, Y. Zhang, S. Liu, J. Chen, G. Fu and N. Zheng, *ACS Appl. Mater. Interfaces*, 2021, **13**, 52193.
- 55 W. Zhang, R. Qin, G. Fu and N. Zheng, *J. Am. Chem. Soc.*, 2021, **143**, 15882.
- 56 R. Qin, L. Zhou, P. Liu, Y. Gong, K. Liu, C. Xu, Y. Zhao, L. Gu, G. Fu and N. F. Zheng, *Nat. Catal.*, 2020, **3**, 703.
- 57 P. Liu, Y. Zhao, R. Qin, S. Mo, G. Chen, L. Gu, D. M. Chevrier, P. Zhang, Q. Guo, D. Zang, B. Wu, G. Fu and N. F. Zheng, *Science*, 2016, **352**, 797.
- 58 K. Liu, R. Qin, L. Zhou, P. Liu, Q. Zhang, W. Jing, P. Ruan, L. Gu, G. Fu and N. Zheng, *CCS Chem.*, 2019, **1**, 207.
- 59 C. Xu, G. Chen, Y. Zhao, P. Liu, X. Duan, L. Gu, G. Fu, Y. Yuan and N. Zheng, *Nat. Commun.*, 2018, **9**, 3367.
- 60 A. Comas-Vives, C. González-Arellano, A. Corma, M. Iglesias, F. Sánchez and G. Ujaque, *J. Am. Chem. Soc.*, 2006, **128**, 4756.
- 61 P. Liu, Y. Zhao, R. Qin, S. Mo, G. Chen, L. Gu, D. M. Chevrier, P. Zhang, Q. Guo, D. Zang, B. Wu, G. Fu and N. Zheng, *Science*, 2016, **352**, 797.
- 62 A. Dedieu, S. Humbel, C. Elsevier and C. Grauffel, *Theor. Chem. Acc.*, 2004, **112**, 305.
- 63 D. Massiot, F. Fayon, M. Capron, I. King, S. Le Calvé, B. Alonso, J.-O. Durand, B. Bujoli, Z. Gan and G. Hoatson, *Magn. Reson. Chem.*, 2002, **40**, 70.
- 64 G. Kresse and J. Hafner, *Phys. Rev. B*, 1994, **49**, 14251.
- 65 G. Kresse and J. Hafner, *Phys. Rev. B*, 1993, **48**, 13115.
- 66 G. Kresse and J. Furthmüller, *Comput. Mater. Sci.*, 1996, **6**, 15.
- 67 G. Kresse and J. Furthmüller, *Phys. Rev. B*, 1996, **54**, 11169.
- 68 G. Kresse and D. Joubert, *Phys. Rev. B*, 1999, **59**, 1758.
- 69 G. Kresse and J. Hafner, *Phys. Rev. B*, 1993, **47**, 558.
- 70 H. J. Monkhorst and J. D. Pack, *Phys. Rev. B*, 1976, **13**, 5188.

